EMPIRICAL DAMAGE AND LIQUEFACTION FRAGILITY CURVES FROM 2012 EMILIA EARTHQUAKE DATA

Di Ludovico M.[1], Chiaradonna A.[2], Bilotta E. [2], Flora A. [2], Prota A. [1]

[1]University of Naples Federico II, Department of Structure for Engineering and Architecture, via Claudio 21,
80125, Naples, Italy
[2]University of Naples Federico II, Department Civil, Architectural and Environmental Engineering, via Claudio 21,
80125, Naples, Italy

The study focuses on the effects of liquefaction on structures taken from data on about 1,000 private residential masonry buildings located in several municipalities struck by the 2012 Emilia earthquake. Survey data were collected by teams of experts coordinated by the Italian Department of Civil Protection in the immediate post-earthquake emergency phase. They included information on building characteristics and the level and extent of the damage to structural and non-structural components. Furthermore, according to data related to the reconstruction process, information on the liquefaction-induced type and extent of the damage was also collected. Through a comparative analysis of the empirical damage, it was found that liquefaction strongly affected the buildings, confirming its relevance in the damage scenario under specific subsoil conditions. Based on this evidence, the paper proposes a correlation between structural damage and liquefaction when it comes to deriving proper preliminary empirical fragility curves. A suitable parameter to define liquefaction effects at ground level is introduced and correlated to damage grades defined according to the European Macroseismic Scale: EMS-98.

INTRODUCTION

Liquefaction may become a major source of seismic risk for structures and infrastructures when loose and saturated sandy soil layers are shallow enough to affect the behavior of buildings via either loss of bearing capacity, potential for lateral spreading, liquefaction induced settlements. Severe structural damage induced by liquefaction has occurred over time during the earthquakes in Anchorage (USA, 1964), Niigata (Japan, 1964), Kobe (Japan, 1995), Kocaeli (Turkey, 1999), Christchurch (New

Zealand, 2010 - 2011), Emilia-Romagna (Italy, 2012) and, more recently, Hualien (Taiwan, 2018) and Palu (Indonesia, 2018). The effects of liquefaction on the buildings in these areas were catastrophic, with rotations of entire structural complexes leading to a loss of functionality and operative state (Tokimatsu et al. 1996; Yoshida et al. 2001; Cubrinovski 2013; Fioravante et al. 2013; Chiaradonna et al. 2018b). Consequently, a great effort was made to understand building movements on shallow foundations using centrifuge testing and numerical modeling (Balakrishnan and Kutter 1999; Kutter et al. 2004; Karamitros et al. 2013; Bray and Dashti 2014, Bouckovalas et al. 2015; Hayden et al. 2015; Allmond et al., 2015; Adamidis and Madabhushi 2018; Hughes and Madabhushi 2019). In detail, Dashti and Bray 2013 individualized possible liquefaction-induced displacement mechanisms in three different typologies: (a) volumetric strains caused by water flow in response to transient gradients; (b) partial bearing failure due to soil softening; and (c) soil-structure-interaction-induced building ratcheting during earthquake loading. Nevertheless, most of the research was devoted to soil-structure-interaction studies on individual buildings, and these are strictly dependent on the specific case under study, e.g., the type of structure and foundation system (Luque and Bray 2017). Very little research has been conducted on fragility curves related to soil liquefaction. Zhang et al. (2008), however, derived fragility functions for different classes of typical bridges in California when subjected to seismic shaking or liquefaction-induced lateral spreading. Lopez-Caballero and Khalil (2018) assessed numerically the effect on a levee of the liquefaction-induced settlement of the soil foundation in terms of analytical fragility curves constructed on the basis of a nonlinear dynamic analysis. Furthermore, using a database of buildings affected by liquefaction during the 2010 Mexicali, 2010 New Zealand and 2011 Japan earthquakes, and with reference to building damage, Cazares et al. (2012) proposed vulnerability functions that are obtained as a result of a combination of the functions defined as empirical and those obtained through damage statistics.

Several approaches have been developed in the literature for correlating types of damage with seismic intensity parameters through a fragility curve. There are methods based on simplified mechanism-based procedures (Cosenza et al. 2005; Borzi et al. 2008), capacity spectrum methods (Iervolino et al. 2007; Del Gaudio et al. 2015), and displacement-based methods (Calvi 1999; Crowley et al. 2004; Borzi et al. 2008). There is, however, also a group of methods based on empirical observations of the expected damage suffered during seismic events (Rota et al. 2008, Del Gaudio et al. 2017).

In the current study, the structural and non-structural damage caused to masonry buildings is analyzed and empirical fragility curves are produced using observational damage data collected after the 2012 Emilia earthquake (section 2). Starting from an analysis of the structural damage described in AeDES forms (Baggio et al. 2007), it has been possible to carry out both a qualitative and quantitative analysis of the observed damage (section 3). In this way, the damage has been subsequently correlated with a

new parameter characterizing the liquefaction phenomenon. Different methodologies for estimating fragility functions from data on damage grades and the parameters of potential liquefaction are illustrated, discussed and applied to the database, leading to the derivation of EMS-98-based fragility curves (section 4).

RECONSTRUCTION PROCESS AND DATA COLLECTION ON DAMAGED BUILDINGS

This section presents the reconstruction procedure and data collected after the 2012 Emilia-Romagna earthquake. At the beginning, reconstruction process ordinances involved residential buildings: Ordinance n. 29, 2012 for temporarily or partially unusable buildings; Ordinance n. 51, 2012 for unusable buildings that have suffered severe damage; and Ordinance n. 86, 2012 for severely damaged buildings requiring a seismic strengthening intervention or demolition and reconstruction. For the first time in Italy, it was also possible to obtain grants for improving the foundation soil. An increased economic contribution for reconstruction up to 15% of the total grant was provided in the areas affected by liquefaction. Note that a specific documentation, aiming at certify liquefaction effects, was required to obtain such extra funding. Moreover, microzonation studies were carried out in the areas struck by the seismic events in order to identify and delimit areas with homogeneous seismic behavior, distinguishing the areas susceptible to the amplification of seismic motion and those susceptible to liquefaction.

Several municipalities were affected by liquefaction, including: Cavezzo; Bondeno; Cento; Pieve di Cento; the hamlet of San Carlo in Sant'Agostino; and Mirabello (Gruppo di lavoro RER, 2012). The data related to liquefaction sites were collected and subsequently georeferenced in the GIS environment (Morga et al. 2018; Spacagna et al. 2018). Figure 1a shows the spatial distribution of cases affected by liquefaction (black squares), with a ShakeMap superimposition related to the event of May 20, 2012.

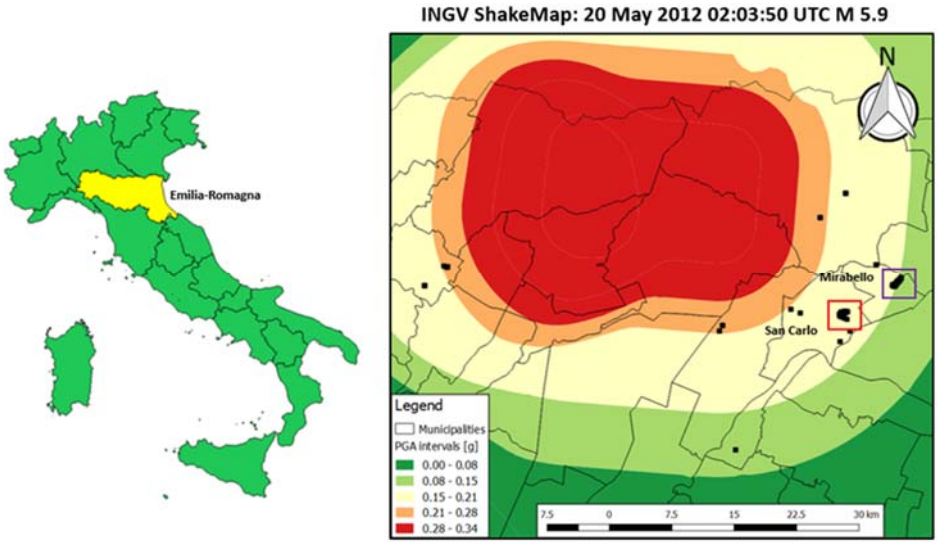

(a)

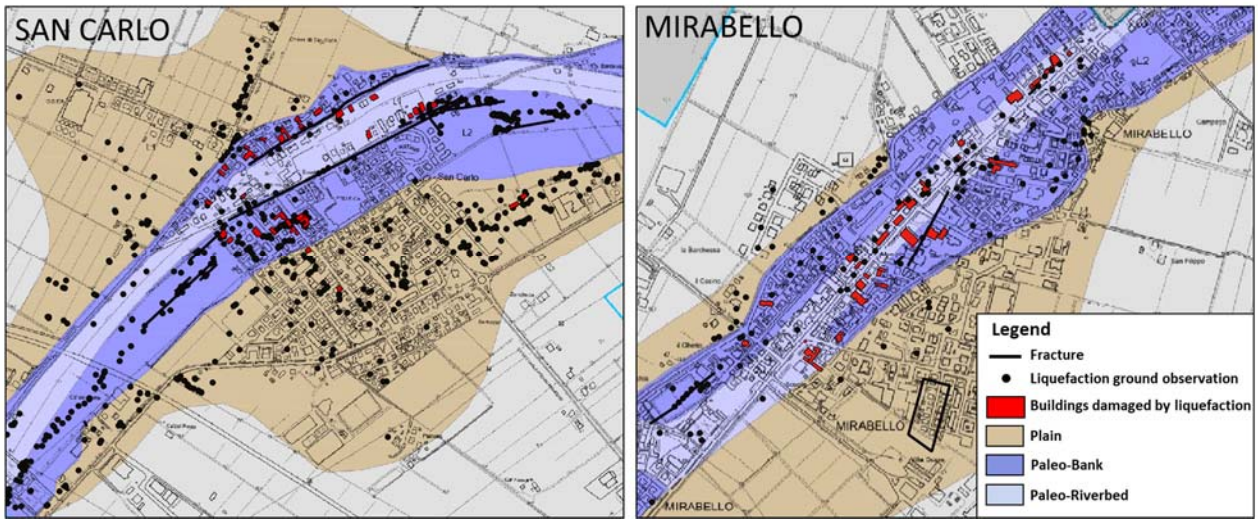

(b) (c)

Figure 1: ShakeMap (http://shakemap.rm.ingv.it/shake/index.html) representing the spatial distribution of peak ground acceleration (PGA) and the buildings affected by liquefaction (**a**); San Carlo (**b**) and Mirabello (**c**) dataset with geological maps and liquefaction evidences.

The peak ground acceleration (PGA) in the area under investigation ranged between 0.0 to 0.34 g. The overlap with the spatial distribution of the liquefaction cases allowed us to see that most buildings fall within an acceleration range of 0.15 to 0.21 g. The distribution of the sites affected by liquefaction is concentrated in the areas related to the municipalities of San Carlo and Mirabello (Modoni et al. 2019). Since most of the buildings affected by liquefaction are located in these two municipalities, the present study will only refer to them. Figures 1b and 1c show a comparison between the distributions of liquefaction evidences and the geological maps of the two considered municipalities. It can be observed that most of the liquefaction manifestations occurred along paleo-river beds and

paleo-channel systems originating from the depositional activity of the Reno river (Facciorusso et al. 2012).

In order to investigate the effects of liquefaction on the behavior of structures, data related to masonry residential buildings located in San Carlo and Mirabello were collected. In detail, two sets of samples were identified and divided into two classes: a) a sample of structures not damaged by liquefaction (these structures may rest on soils that did not liquefy or that liquefy at depth without any consequence for the foundations; in the following these cases will be referred to as structures not damaged by liquefaction – NDL); and b) a sample of structures damaged by liquefaction (DL). Table 1 shows the frequencies of the samples.

Table 1: Number of masonry buildings from ISTAT 2011 and for NDL – DL samples.

		MUNICIPALITY		**Total**
		MIRABELLO	SAN CARLO	
No. of masonry buildings	Census (ISTAT2011)	675	439	1114
	NDL buildings	277	373	650
	DL buildings	55	46	101

The number of buildings was also compared with the masonry residential buildings contained in the census data (ISTAT 2011). It was assumed that buildings without a usability request (1114-650-101 = 363) did not suffer any structural damage. This hypothesis is reliable since requests for the evaluation of building usability were made by owners via the AeDES forms after the earthquake. Accordingly, the lack of data obtained from in situ inspections mainly means that no damage was suffered by these buildings.

The data contained in the AeDES forms were used to make an initial comparison between the NDL and DL buildings, in terms of construction age, number of floors, average story surface area, and masonry quality. These macro-parameters may greatly affect building behavior in case of seismic events and were thus analyzed to verify if they play a crucial role in defining the different empirical damage detected in the NDL and DL buildings. Indeed, the construction age allows defining the building type of design (i.e., for gravity loads only or with reference to obsolete or current seismic design rules), number of floors and surface area strongly affect the structural fundamental period of vibration and thus its behavior under seismic actions, and masonry quality determine the capacity of structural components to sustain horizontal actions provided by seismic events.

131 Figure 2 reports the frequency and cumulative percentage of the two classes of structure, i.e., NDL
132 and DL (751 buildings) as a function of the construction age, number of stories and average story
133 surface area. The construction age was classified according to eight periods (before 1919, between
134 1919 and 1945, 1946-1961, 1962-1971, 1972-1981, 1982-1991, 1991-2001, and after 2001), as
135 commonly adopted in the census data (and the AeDES forms). The trend of the cumulative percentage
136 was similar. Figure 2a shows that 82.6% of the NDL building dataset (corresponding to 455 buildings)
137 and 73.3% of the DL building dataset (corresponding to 92 buildings) were built before 1971. The
138 graph in Figure 2b shows that about 98% of the buildings in the datasets (corresponding to 635
139 buildings for the NDL class and 99 buildings for the DL class) had between one and three stories.
140 Finally, Figure 2c highlights that about 40% of the buildings (corresponding to 365 buildings for the
141 NDL and 63 buildings for the DL classes) had an average story surface area between 70-100 and 170-
142 230 m^2.
143 Consequently, it was possible to assume that the two classes are comparable in terms of the macro-
144 parameters affecting the structural vulnerability to seismic action. Moreover, the data related to the
145 quality of the masonry revealed a percentage of buildings of good quality and with regular texture
146 masonry (77% and 61% for the NDL and DL classes, respectively).
147

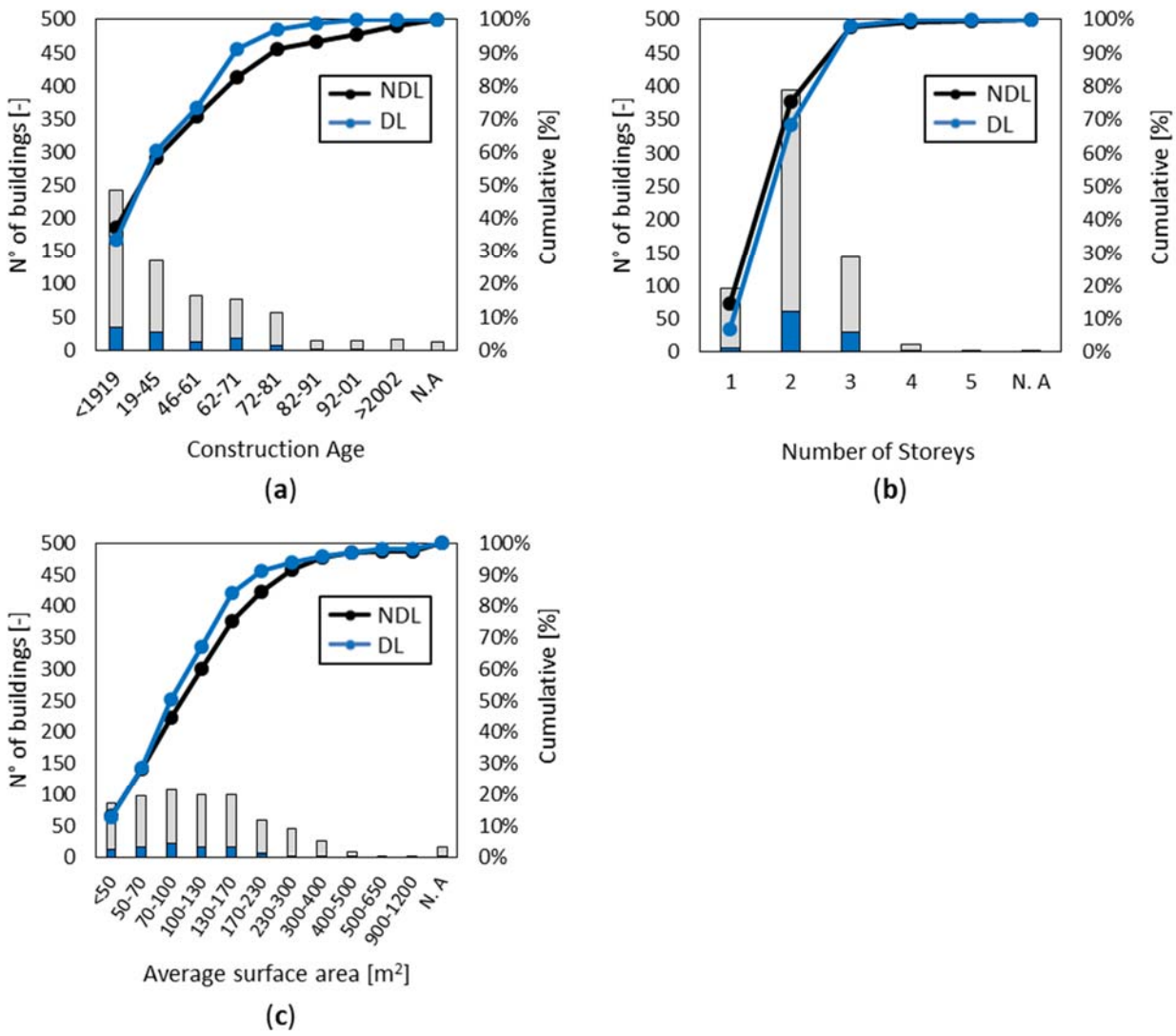

Figure 2: Distribution and cumulative percentage of the no damaged by liquefaction NDL and damaged by liquefaction DL buildings as a function of the construction age (**a**), number of stories (**b**) and average story surface area (**c**).

ANALYSIS OF LIQUEFACTION-INDUCED DAMAGE

In the post-Emilia earthquake reconstruction process, documentation was required to: illustrate the damage sustained; describe the interventions needed to achieve building usability; and quantify the financial support sought from the government. The documentation related to the DL buildings shows that the typical damage caused by foundation settlement largely occurred in buildings that were also damaged by inertial effects (i.e., seismic effects on the superstructure). In particular, according to the observed damage, it can be assumed that in this case liquefaction was activated at different stages of

the seismic event at different sites, even if relatively close. The different behavior mostly depends on local conditions in terms of liquefiable soil layer density and thickness.

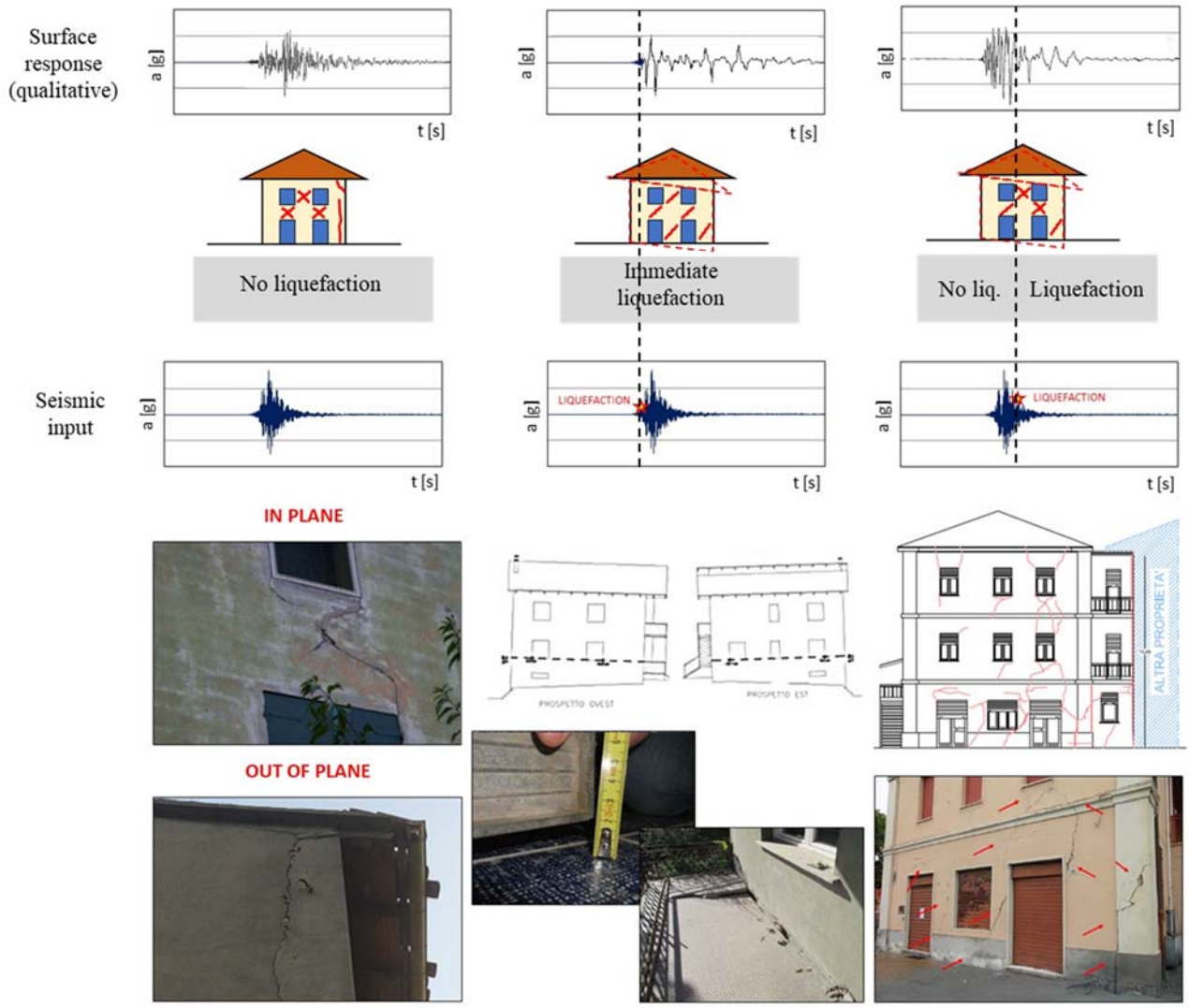

(**a**) (**b**) (**c**)

Figure 3: Empirical damage observed in the case of: no soil liquefaction (**a**); early liquefaction activation (**b**); combined inertial and liquefaction effects (**c**).

Figure 3 schematically represents three possible conditions related to the absence of liquefaction (Figure 3a), or the attainment of liquefaction at different stages (figures 3b, c). The figure also reports the type of structural damage commonly detected in Mirabello and San Carlo in such three cases. In the case of no liquefaction (Figure 3a), failures due to the out-of-plane mechanisms of walls or in-plane diagonal cracks (inclined at about ±45°) are commonly detected in the structures. In the case of seismic events that suddenly activate liquefaction or in the case of liquefaction activated for accelerations much lower than the PGA (Figure 3b), the effects are mainly related to liquefaction. The common failures in such a case are rigid building rotations, with a relevant loss of functionality

of the structure, as well as one-way diagonal cracks due to foundation settlements. Damage caused by inertial forces is mostly absent, because liquefaction works as a natural isolation system for the superstructure. Finally, Figure 3c shows the combined effects of soil liquefaction and inertial forces on the buildings, which are due to significant inertial forces on the superstructure and liquefaction-induced damage. With the current state of knowledge, it is very difficult to predict when liquefaction is activated, because it is very dependent on the characteristics of the soil.

Comparative analysis of empirical damage: NDL vs. DL buildings

A comparative analysis of the previously described damage to the NDL and DL buildings is carried out herein using data from AeDES forms. In particular, the data refer to the severity and extent of the damage detected in: vertical structural components (VS), (e.g., masonry vertical bearing walls); floors (F); stairs (S); roofs (R); and infill-partitions (IP). The AeDES forms identify four damage levels for each structural or non-structural component: no damage, D0; slight damage, D1; medium-severe damage, D2-D3; and very heavy damage or collapse, D4-D5. The observed damage level definition is based on the European Macroseismic Scale EMS98, integrated with the definitions used in the GNDT survey form, GNDT 1993, Baggio et al. 2007, (Grünthal 1998).

The damage extent is reported as follows: damage extent less than 1/3; between 1/3 and 2/3; and greater than 2/3 of the storey components. Figure 4 shows a comparison between the DL and NDL buildings in terms of cumulative damage probability matrices (C-DPMs) that represent the percentage of buildings that reaches or exceeds the j-th level of damage in VSs.

The figure clearly shows that the DL-class buildings suffered damage to the VSs that was more severe than that observed in the NDL sample. The data related to other structural or non-structural components are summarized in Table 2 and confirm that the severity and extent of the damage detected in the DL buildings was greater than that in the NDL buildings, especially with reference to stairs.

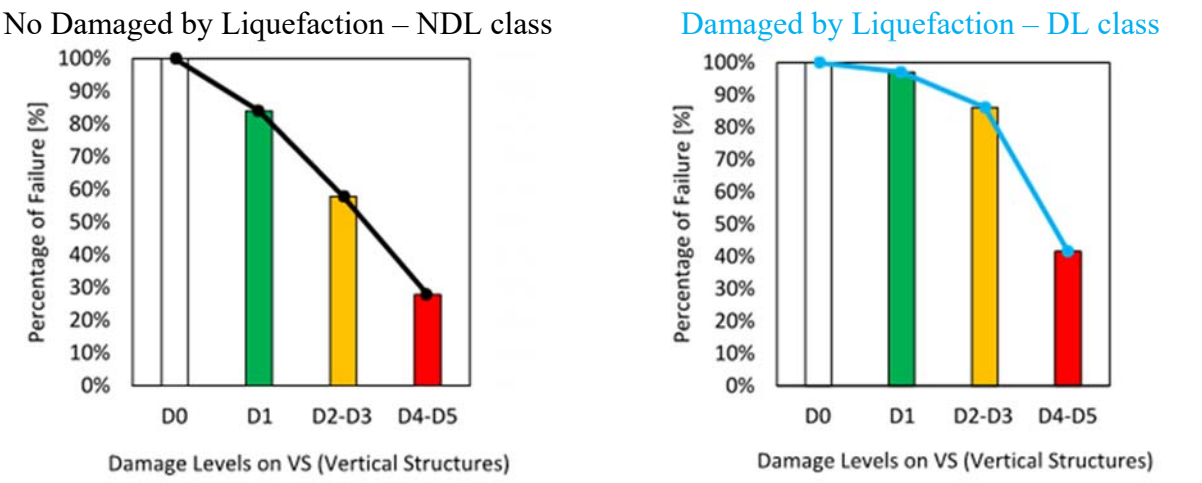

Figure 4: Vertical structure (VS) - C-DPMs: NDL class (a); DL class (b).

Table 2: Cumulative percentage of failure expressed as a function of the damage levels in the other structural components for both the NDL and DL samples.

	D1		D2-D3		D4-D5	
	NDL	DL	NDL	DL	NDL	DL
VS	84.0%	97.0%	57.8%	86.1%	27.8%	41.6%
F	62.5%	84.2%	35.7%	47.5%	22.8%	26.7%
S	36.6%	66.3%	27.2%	44.6%	21.7%	29.7%
R	52.0%	72.3%	35.7%	48.5%	24.3%	34.7%
IP	70.2%	92.1%	35.5%	51.5%	20.9%	26.7%

Effects of structural vulnerability on empirical damage

In order to analyze the effects of structural vulnerability on the empirical damage detected in the NDL and DL buildings, different subsets of buildings for each class are defined in this section according to data related to vertical and horizontal structure types. In particular, Section 3 of the AeDES forms (Baggio et al. 2007) identifies five vertical structure types: a) unknown; b) masonry with an irregular layout or bad quality without ties; c) masonry with an irregular layout or bad quality with ties; d) masonry with a regular layout or good quality without ties; and e) masonry with a regular layout or good quality with ties. Furthermore, six horizontal structure types are reported: a) unknown; b) vaults with no ties; c) vaults with ties; d) beams with flexible slabs; e) beams with semi-rigid slabs; and f) beams with rigid slabs. Neglecting unknown structural types, the combination of vertical and

horizontal structures leads to 20 masonry subsets of buildings, representing different vulnerability categories. Table 3 summarizes the number of buildings in each subset related to the NDL and DL classes, respectively. Note that the total number of buildings is slightly lower than that reported in Table 1 because, in a few cases, the "unknown" structural type was selected in the AeDES form. A mean empirical global damage factor,μ_D, has been computed for each subset as the mean value of the global damage related to each building, $\mu_{D,i}$, defined as:

$$\mu_{D,i} = \sum_j D_j \gamma_j \quad (1)$$

where D_j is the damage level and extent related to the j^{th} component (j=VS, F, S, R and IP), and γ_j is a coefficient, ranging between 0 and 1, accounting for the weight of the damage on the j^{th} component. D_j is computed as:

$$D_j = \frac{\sum_{D=D0}^{D5} D \cdot e_{k,D}}{5} \quad (2)$$

where D is the damage level (D0=0, D1=1, D2-D3=2.5, D4-D5=4.5) and $e_{k,D}$ is a coefficient accounting for the damage extent of the damage level D; $e_{k,D}$ can assume three values depending on the percentage of the building affected by damage, k: k < 1/3, $e_{k,D} = 0.17$; k between 1/3 and 2/3, $e_{k,D} = 0.5$; and k>2/3, $e_{k,D} = 0.83$) (Dolce et al. 2001).

Table 3: Number of buildings in 20 subsets of NDL and DL buildings according to the horizontal and vertical structure type.

Vertical structure (masonry walls) / Horizontal structure (floor and beams)	Masonry structural units				Total
	Irregular layout or bad quality		Regular layout or good quality		
	w/o tie rods or tie beams	with tie rods or tie beams	w/o tie rods or tie beams	with tie rods or tie beams	
Vaults without tie rods	1 (-)	- (-)	2 (-)	2 (-)	**5 (-)**
Vaults with tie rods	- (-)	- (-)	3 (-)	5 (1)	**8 (1)**
Beams with flexible slabs	53 (16)	9 (1)	187 (19)	28 (4)	**277 (40)**
Beams with semi-rigid slabs	24 (8)	1 (-)	107 (18)	32 (7)	**164 (33)**
Beams with rigid slabs	2 (2)	2 (-)	40 (5)	96 (8)	**140 (15)**
Total	**80 (26)**	**12 (1)**	**339 (42)**	**163 (20)**	**594 (89)**

* *Black for No Damaged by Liquefaction - NDL subsets; blue for Damaged by Liquefaction- DL subsets*.

Figure 5 reports an overall comparison between the mean damage, μ_D, suffered by the different subsets of data for the NDL (Figure 5a) and DL (Figure 5b) buildings, respectively. The number of buildings required to compute the mean global damage of each subset is also reported in Figure 5 as well as the median value of damage for each subset and the dispersion (i.e. 16th and 84 percentile). Figure 5a shows a very similar value of μ_D (i.e., in the range 0.10 -0.20) for masonry buildings with vaults with or without tie rods or with flexible slabs. However, it should be noted that the data for buildings with vaults are very limited, and this may affect the results. As expected, the mean empirical global damage decreases in the case of buildings with a horizontal structure characterized by semi-rigid or rigid slabs, with values lower than 0.10 for each building subset. This result is consistent with the favourable role of such structural components in the global behavior against seismic action. Indeed, they allow the transfer of seismic actions on VSs leading to a desirable so-called "box-type" building behavior. Furthermore, there is clear evidence of the benefits provided by a regular layout and good quality masonry compared to an irregular layout and bad quality stonework. Accordingly, a clear trend can be observed between the parameters influencing structural vulnerability to lateral actions and the mean empirical global damage. In contrast, Figure 5b clearly shows that the trend between the mean empirical global damage and the vertical/horizontal structural types is less evident than in the NDL building class. This is probably because the liquefaction may induce localized effects or the global rotation of the buildings that are less affected by those structural characteristics. Furthermore, the mean empirical global damage peak value is greater in the DL class buildings than

in the NDL subsets: μ_D = 0.27 versus μ_D = 0.20. However, it should be noted that the number of buildings in each data subset for the DL class is significantly lower than in the NDL subsets and this may influence the results.

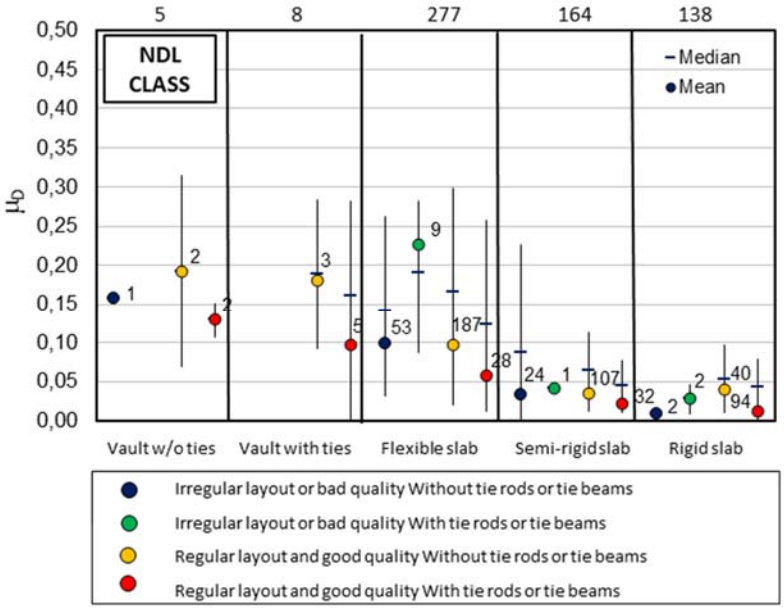

(a) No Damaged by Liquefaction – NDL class

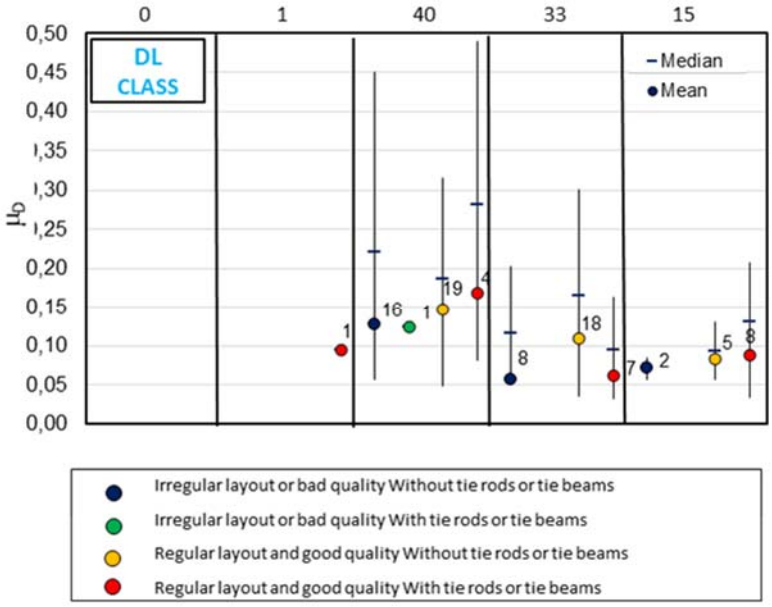

(b) Damaged by Liquefaction – DL class

Figure 5: Mean empirical damage as a function of the vulnerability categories of buildings.

In order to better investigate the influence of masonry texture and quality on the global mean empirical damage, Figure 6 reports a direct comparison of their trend for the NDL and DL building

subsets. In general, the figure shows that the stiffer the horizontal structure is, the better the global structural behavior for both the NDL and DL data subsets. Furthermore, the damage detected to the DL buildings was always greater than that in the NDL buildings.

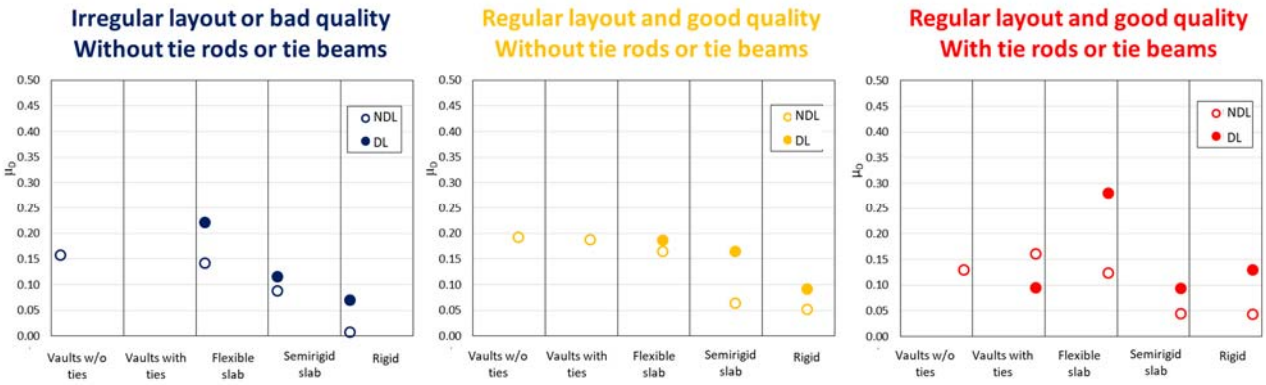

Figure 6: Mean empirical damage; comparison between the No Damaged by Liquefaction – NDL and Damaged by Liquefaction – DL data subsets.

Prediction of repair costs

The mean empirical damage is a measure of the global damage detected in a building, but may not be an adequate measure when it comes to making a prediction of losses, because it does not correlate the damage caused to each building component with its economic value. Indeed, recent studies demonstrated that the repair costs are strongly affected by nonstructural components rather than structural ones (De Martino et al. 2017, Del Vecchio et al. 2018). Consequently, in this section, in order to focus on the impact of liquefaction in terms of economic losses, a different parameter is used to compute these losses, in particular a measure that is related to the aftermath of the L'Aquila event (De Martino et al. 2017). This parameter, named as the damage factor (DF), has been calibrated on data costs related to the reconstruction process and directly accounts for the real losses computed by practitioners involved in the estimation of repair costs (Di Ludovico et al. 2016a and b). The DF is directly computed using the data reported in Section 3 of the AeDES forms, but depends on the D_j and γ_j values specifically calibrated for loss analyses. Furthermore, a relationship between the DF and actual repair costs (ARC) induced by damage (or between the DF and an a-dimensional cost ratio obtained as a ratio between the ARC related to the building and the average building demolition and reconstruction cost - building repair cost ratio, Cr) is reported in De Martino et al. 2017 and recalled as follows:

$$ARC = 143 + 849\,DF - 277\,DF^2 \quad (3)$$
$$C_r = 0.12 + 0.71\,DF - 0.23\,DF^2$$

Figures 7a,b report the DF with a median and 16th and 84th percentiles, as well as the relevant ARC and C_r values for the NDL and DL buildings. The analysis refers to NDL and DL buildings classes rather than the subsets of data analysed in the previous section because it aims capturing the effects of liquefaction on costs rather than structural vulnerability parameters on costs.

The median DFs are 0.052 and 0.124, corresponding to a median Cr of 0.156 and 0.204 for the NDL and DL classes, respectively. Accordingly, the effects of liquefaction may lead, based on the predictions of such a model, to an increase in the repair costs of about 30% in cases where liquefaction was not observed.

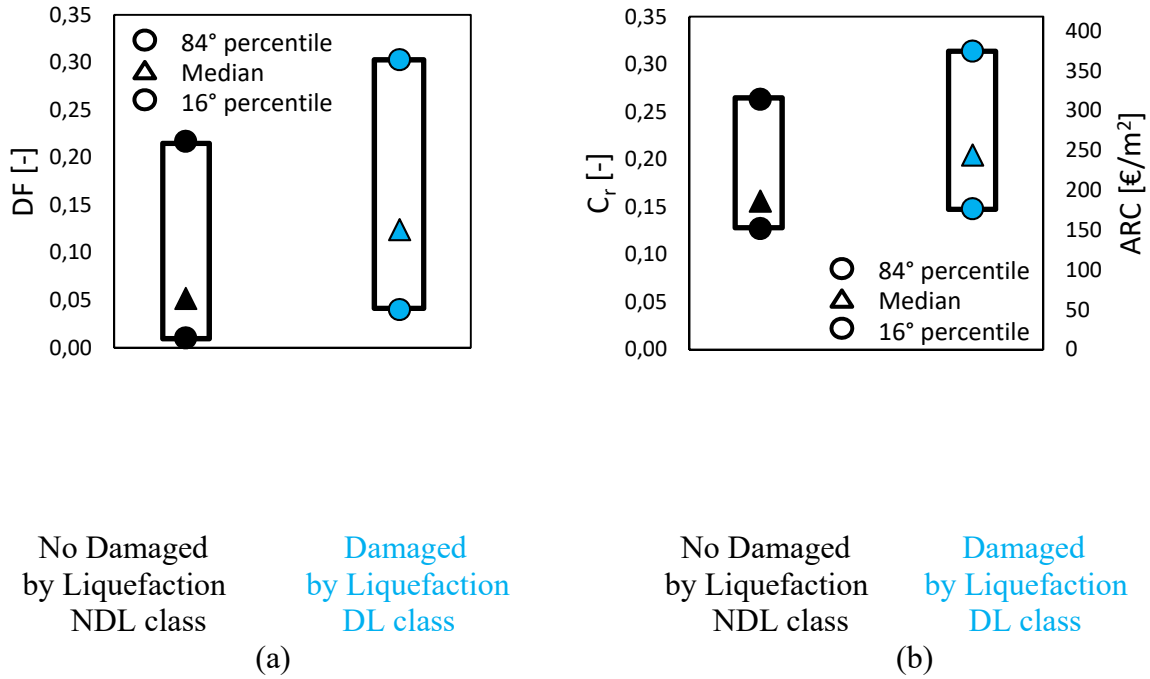

Figure 7: Median, 16th and 84th percentile DFs for the NDL and DL classes (**a**); building repair cost ratio C_r and actual repair costs ARC (**b**) for the NDL and DL classes.

EMPIRICAL FRAGILITY CURVES

Fragility curves related to seismic events define the exceeding probability of a given damage grade (DG) as a function of a ground motion intensity measure (IM). The IM may be a macroseismic parameter or, as commonly adopted in recent studies, is represented by a ground motion intensity record in terms of various peak ground parameters: acceleration (PGA); velocity (PGV); and displacement (PGD). A commonly used functional form and regression technique to produce fragility curves is the lognormal cumulative distribution function:

$$P[DG \geq dg|IM] = \Phi\left(\frac{\ln(IM) - \mu}{\sigma}\right) \quad (4)$$

where $\Phi(\cdot)$ is the standard normal cumulative distribution function (CDF), μ is the logarithmic mean and σ is the logarithmic standard deviation defining the lognormal distribution. This returns values between 0 and 1 and is particularly suitable for fitting data clustered around low values, as is commonly the case in fragility analyses (Rossetto et al. 2013). The parameters σ and μ can be determined according to the nonlinear least squares estimation (LSE) methodology, which aims to derive the most accurate description of data, or by means of the maximum likelihood estimation (MLE) approach (e.g., Baker 2015), which is an iterative method to determine the parameters maximizing the likelihood function:

$$Likelihood = \prod_{j=1}^{m} \binom{N_j}{n_j} p_j^{n_j} (1 - p_j)^{N_j - n_j} \quad (5)$$

where p_j is the probability that n_j number of buildings over N_j shows damage that is greater than or equal to a threshold DG_i in the j^{th} bin of the IM.

Another available functional form used in the literature is the exponential model (Rossetto and Elnashai 2003, Amiri et al. 2007).

$$P[DG \geq dg|IM] = 1 - e^{-\alpha IM^{\beta}} \quad (6)$$

The parameters α and β can be determined according to the LSE or MLE methodology. In the following, both functional forms (i.e. lognormal and exponential) are used, along with the nonlinear LSE and MLE methodologies. In order to produce fragility curves that take into account the liquefaction phenomenon, it is necessary to define suitable DGs and IMs.

Damage grades

The empirical data collected in Section 4 of the AeDES forms (Baggio et al. 2007) were used to define the buildings' DGs. In particular, the DG of each building was determined by accounting for the level and extent of the damage to the VS component, and five damage grades were assumed based

on the European Macroseismic Scale, EMS-98 (Grünthal 1998). The criterion used to convert the damage levels to DGs was that reported in Dolce et al. 2017 and is summarized in Table 4.

Table 4: DG (EMS-98) and corresponding damage levels to VSs according to the AEDES survey forms (Baggio et al. 2007).

Vertical structures			
EMS-98 damage		**AeDES damage**	
Damage grade	Damage description	Damage level	Extent
DG1	*Fine cracks in plaster over frame members or in walls at the base.*	D1	<1/3 1/3-2/3 >2/3
DG2	*Cracks in the columns and beams of frames and in structural walls.*	D2-D3	<1/3
		D2-D3 and D1	<1/3
			<1/3 and 1/3-2/3
			<1/3 and >2/3
DG3	*Cracks in the columns and beam-column joints of frames at the base and at the joints of coupled walls.*	D2-D3 and D1	1/3-2/3 and <1/3
		D2-D3	1/3-2/3 >2/3
		D4-D5	<1/3
		D4-D5 and D1	<1/3 and <1/3
			<1/3 and 1/3-2/3
		D4-D5 and D2-D3	<1/3 and <1/3
		D4-D5 and D2-D3 and D1	<1/3
DG4	*Large cracks in structural elements, with a compression failure of the concrete and a fracture of rebars; […] collapse of a few columns or a single upper floor.*	D4-D5 and D2-D3	<1/3 and 1/3-2/3
			<1/3 and >2/3
		D4-D5	1/3-2/3
		D4-D5 and D1	1/3-2/3 and 1/3-2/3
		D4-D5 and D2-D3	1/3-2/3 and <1/3
DG5	*Collapse of ground floor or parts of buildings.*	D4-D5 and D2-D3	1/3-2/3 and 1/3-2/3
		D4-D5	>2/3
		D4-D5 and D1	>2/3 and <1/3
		D4-D5 and D2-D3	>2/3 and <1/3

The table shows the corresponding DGs assumed for the building for each damage level and its relevant extent. Note that the AeDES forms allow multiple choices in the selection of the damage level and extent and so different combinations are possible.

Potential liquefaction indices

In this study, a liquefaction potential index was adopted as an IM, in order to correlate the observed building damage due to the occurrence of liquefaction.

The assessment of potential liquefaction is still one of the most debated topics in earthquake geotechnical engineering. In common engineering practice, it is usually based on simplified methods which propose empirical relationships between liquefaction evidence observed after strong seismic events and soil liquefaction resistance, as measured with traditional in-situ tests, such as Cone Penetration Tests (CPTs) and Standard Penetration Tests (SPTs) (Boulanger and Idriss 2016). Within this framework, it is possible to calculate a safety factor against liquefaction triggering, F_L, for each of the investigated layers as the ratio between the soil liquefaction capacity, CRR, and the expected seismic demand, CSR. The increased attention paid to the effects on the built environment induced by liquefaction has led over time to the introduction of indices expressing the severity of the effects at ground surface of soil liquefaction occurring in depth. The earliest index was proposed by Iwasaki et al. 1984 as a function of the safety factor F_L against liquefaction and is as follows:

$$LPI = \int_0^{20} F(z) \cdot W(z) dz \tag{7}$$

where z is the depth of the midpoint of the soil layer in meters and $F(z)$ and $W(z)$ are:

$$F(z) = \begin{cases} 1 - F_L & \text{for } F_L < 1 \\ 0 & \text{for } F_L \geq 1 \end{cases} \tag{8}$$

$$W(z) = 10 - 0.5z \tag{9}$$

Although it has gained wide popularity worldwide, the LPI only accounts for conditions of full liquefaction ($F_L \leq 1$), while excess pore pressure build-up can induce a significant reduction in stiffness and strength of soil also when liquefaction condition has not been attained. Such excess pore pressure build-up induces settlement, while the reduction of shear strength reduces the bearing capacity safety margins prior to liquefaction triggering. Furthermore, even in these non-liquefied conditions, the post-seismic consolidation process (possible if the stratigraphic conditions allow for drainage) leads to settlement at ground level (Spacagna et al. 2017; Chiaradonna et al. 2018a). Over the years, modifications to the LPI have been proposed by several authors (Sonmez 2003; Sonmez and Gokceoglu 2005; Rashidian and Gillins 2018). Sonmez & Gokceoglu (2005), for instance, introduced a liquefaction probability in the original formulation. However, the threshold value of the safety factor that they introduce in the analysis is still a debated issue.

Recently, Van Ballegooy et al. (2014) introduced a new parameter, named liquefaction severity number (LSN). This parameter is calculated by considering soil volumetric deformation, and has the advantage of allowing the contribution of unliquefied $(F_L \geq 1)$ soil strata to be taken into account, thus removing one of the shortcomings of LPI. Even though this correlation is easy to use, it has the major drawback of being based on laboratory test results obtained on a specific sand (Fuji River sand). A completely different approach to take into account the effect of liquefaction at ground level has been proposed by Ishihara (1985), who suggests to correlate in a qualitative way to the onset of damage the thickness of the superficial crust and of the liquefiable layer, as well as the maximum ground acceleration, using the chart reported in Figure 8.

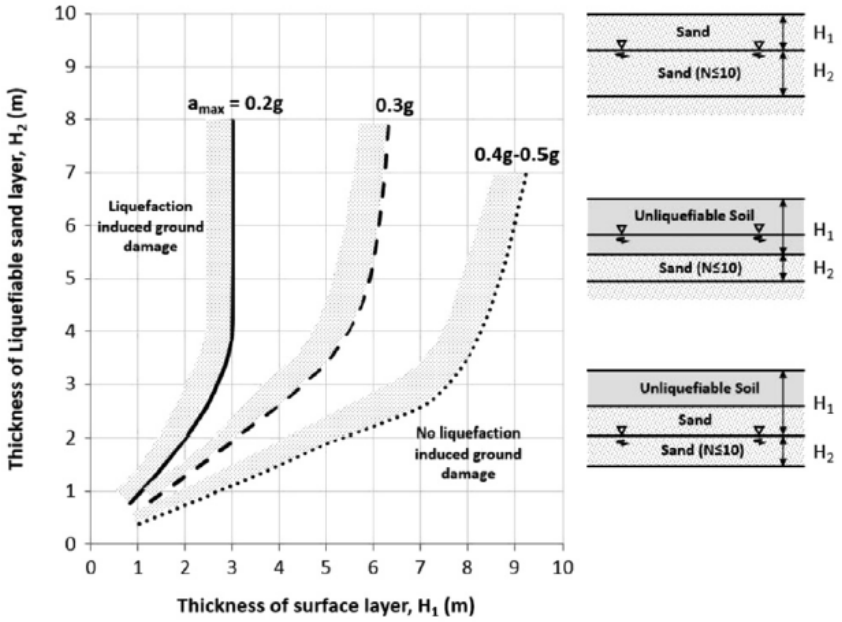

Figure 8: Relationship between thickness of a liquefying, H_2 (m) and thickness of a non-liquefying overlying layer, H_1 (m) at sites for which surface manifestation of level-ground liquefaction has been observed (modified after Ishihara 1985)

This approach is intriguing because directly links the observed damage to the most relevant variables related to liquefaction induced settlements, which should be preferred in the definition of an integral parameter to the safety factor adopted by the other approaches (LPI, LSN, etc.).

Therefore, in this work an estimate of the liquefaction induced settlement has been used to derive an IM to be adopted for defining the fragility curves. As the effects of sand ejecta (if any) are difficult to quantify, the post-consolidation settlement was specifically considered. In free-field conditions, such a settlement can be expressed as:

$$w = \int_{z_{min}}^{z_{max}} \frac{\Delta\sigma'_v(z)}{E_{oed}(z)} dz \tag{10}$$

where z_{min} and z_{max} are, respectively, the minimum and maximum depths of the uppermost saturated, potentially liquefiable, soil layer (Figure 9); $\Delta\sigma'_v$ is the increase of effective vertical stress induced by the dissipation of the excess pore pressure, Δu; and E_{oed} is the constrained (oedometric) modulus.

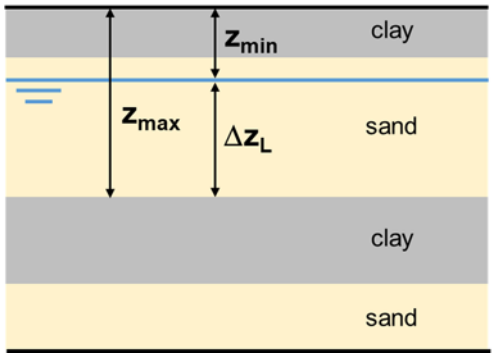

Figure 9: Minimum, z_{min}, and maximum, z_{max}, depths of the uppermost saturated, potentially liquefiable, soil layer.

A new liquefaction potential index, Induced dAmage Measurement, is then proposed as IM in this work:

$$I_{AM} = \frac{1}{1 + z_{min}} \cdot \int_{z_{min}}^{z_{max}} r_u \cdot dz \tag{11}$$

in which r_u is the excess pore pressure ratio (defined as the ratio between the excess pore pressure induced by the seismic event, Δu, and the initial effective vertical stress in free-field conditions, σ'_{v0}). This index was adopted because it is strictly related to the volumetric settlement of ground level induced by liquefaction, as will be shortly discussed in the following. Using the parameter r_u, equation (10) can be written as:

$$w = \int_{z_{min}}^{z_{max}} \frac{r_u \cdot \sigma'_{v0}(z)}{E_{oed}(z)} dz \tag{12}$$

Assuming for $\sigma'_{v0}(z)$ and $E_{oed}(z)$ the mean values $\sigma'_{v0,m}(z = (z_{min} + z_{max})/2)$ and $E_{oed,m}(z = (z_{min} + z_{max})/2)$, eq. (12) can be rearranged as:

$$\frac{w \cdot E_{oed,m}}{\sigma'_{v0,m}} = \int_{z_{min}}^{z_{max}} r_u \, dz \tag{13}$$

In order to make this normalized settlement non-dimensional, and considering that the potential post-liquefaction settlement is more likely to take place as this layer gets closer to ground level, the desired

(and physically based) parameter I_{AM} defined by eq. (11) is finally obtained from eq. (13) dividing it for $(1+z_{min})$.

In a fully liquefied layer (r_u=1), the expression of I_{AM} simplifies and becomes:

$$I_{AM} = \frac{w \cdot E_{oed,m}}{\sigma'_{v0,m} \cdot (1 + z_{min})} = \frac{\Delta z_L}{1 + z_{min}} \quad (14)$$

The simplified expression of I_{AM} (eq. 14) can be simply calculated on the basis of stratigraphic evidence, and is then best fitted for the investigation of wide areas.

The proposed potential index has been computed for both study areas based on the field investigation database produced by the Emilia Romagna region, which is composed of 166 CPTs and 170 CPTUs. In this case the simplification r_u=1 was based on the results of 1D numerical analyses in effective stress (using the code SCOSSA, Tropeano et al. 2019) carried out on representative soil profiles for San Carlo and Mirabello using the seismic input obtained by deconvolution of the Mirandola record (MRN) of the 20 May 2012 Emilia Earthquake (Chiaradonna et al. 2018b). These results indicate that full liquefaction of the uppermost liquefiable layer was extensively reached in the paleo-riverbed and in the paleo-bank (Figure 1) (Caputo et al. 2019), as shown for example in Figure 10.

This simplified assumption is realistic, since there was widespread evidence of liquefaction in the study area (Fioravante et al. 2013; Lai et al. 2015; Papathanassiou et al. 2015).

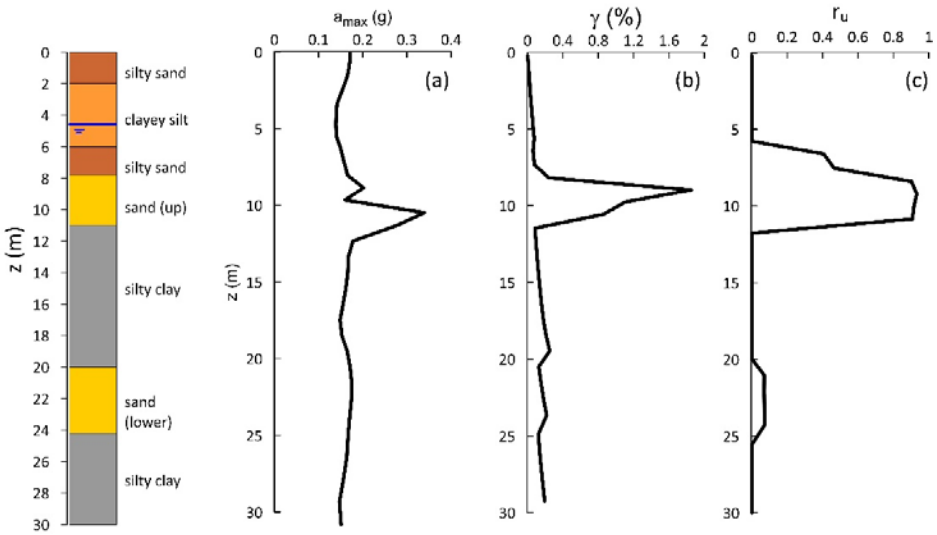

Figure 10: Example of 1D numerical analysis carried out in San Carlo, showing full liquefaction of the uppermost sand layer (sand(up)) (modified after Caputo et al. 2019).

Figure 11 shows the minimum depth isolines of the first potentially liquefiable soil layer under the surface, z_{min} (in meters), superimposed on the geological map. The figure highlights that the liquefiable soil deposits are shallowest along the paleochannel and paleobank (depth of 2-3 m on average), while higher depths are observed in the surrounding plain.

The spatial distribution of the thickness of the potential liquefiable soil, Δz_L (in meters), is also shown in Figure 12. The thicker liquefiable deposits, 6 m on average, are observed along the paleo-channel and paleo-bank, which are confirmed as the areas that are most susceptible to liquefaction.

Finally, Figure 13 reports the spatial distribution of the proposed index, according to eq. (15), which is consistent with the geological setting and the observed damage. As a matter of fact, higher I_{AM} values are calculated along the paleo-channel of the Reno River in both municipalities, where most of the DL buildings are also located.

Since the I_{AM} distribution reflects the geological map of the area (Figure 13), a mean I_{AM} value has been assigned to any geological unit, as reported in Figure 14.

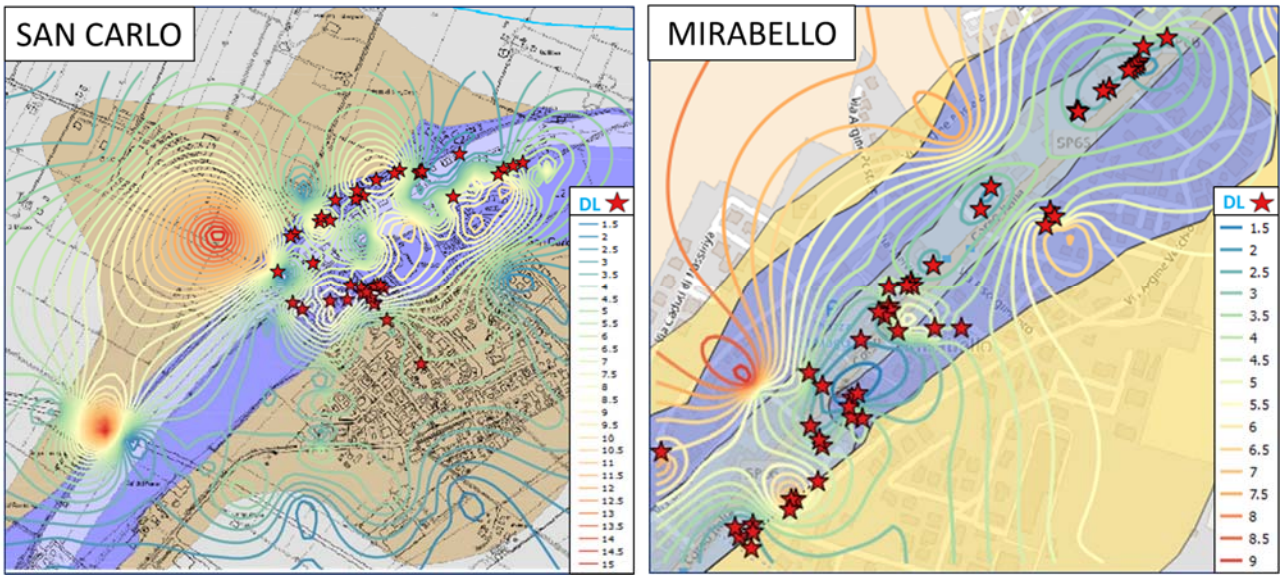

(**a**) (**b**)

Figure 11: Minimum depth isolines of the first potentially liquefiable soil layer under the surface, z_{min} (in meters), superimposed on the geological map, vs. the observed building damage induced by liquefaction (red symbols) in the municipalities of San Carlo (**a**) and Mirabello (**b**).

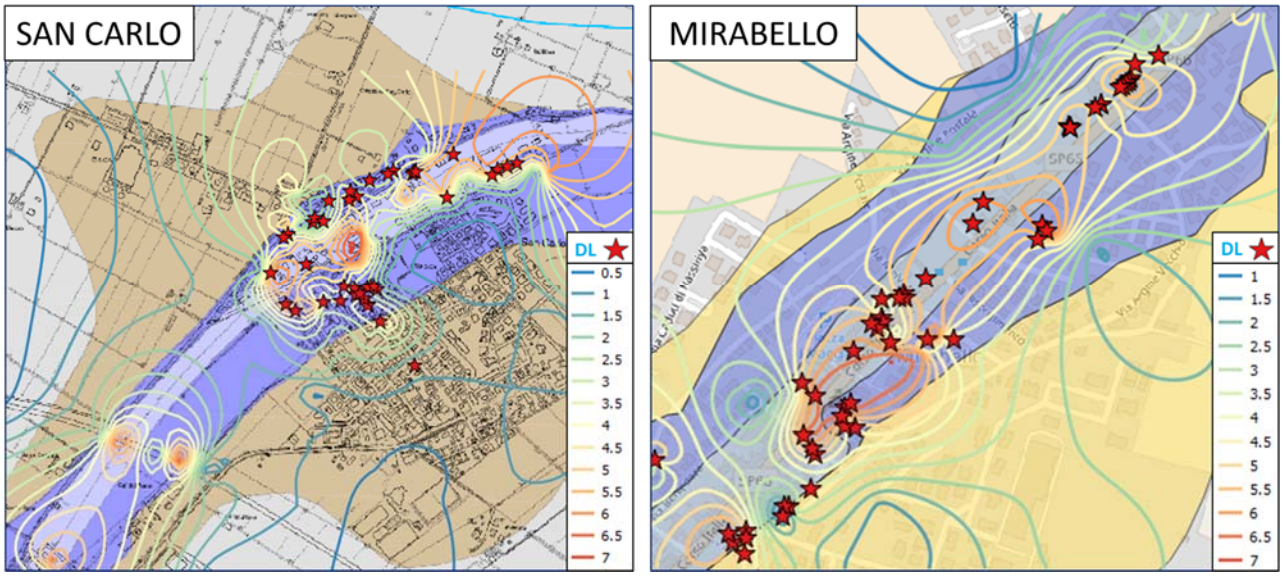

(**a**) (**b**)

Figure 12: Thickness isolines of the potentially liquefiable soil, Δz_L (in meters), superimposed on the geological map, vs. the observed building damage induced by liquefaction (red symbols) in the municipalities of San Carlo (**a**) and Mirabello (**b**).

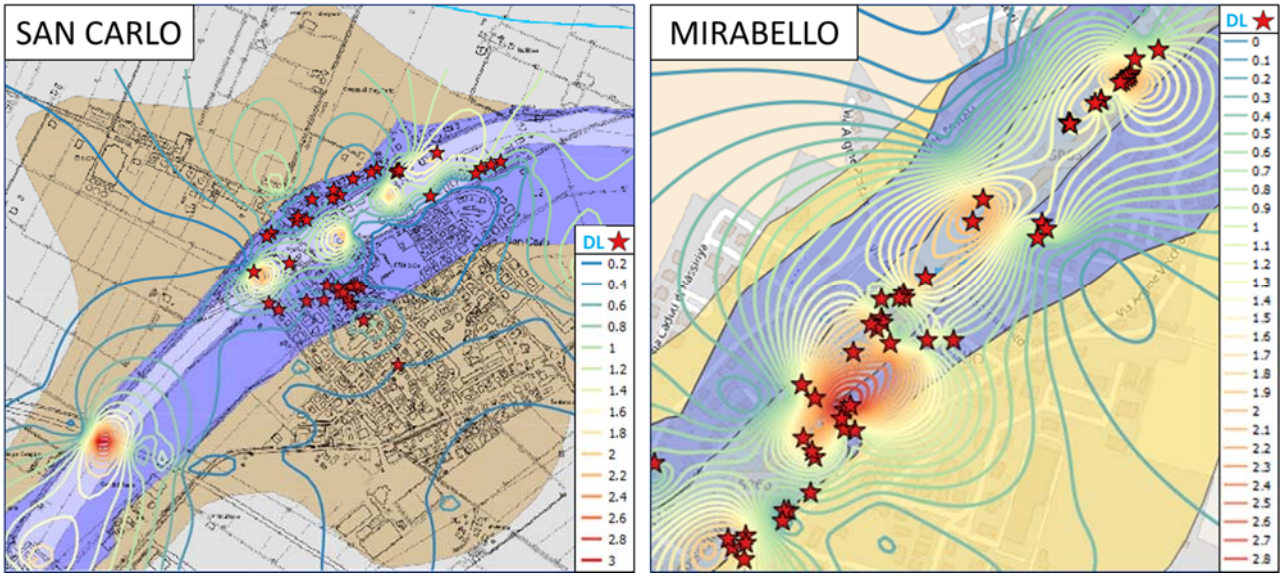

(**a**) (**b**)

Figure 13: I_{AM} index isolines superimposed on the geological map, vs. the observed building damage induced by liquefaction (red symbols) in the municipalities of San Carlo (**a**) and Mirabello (**b**).

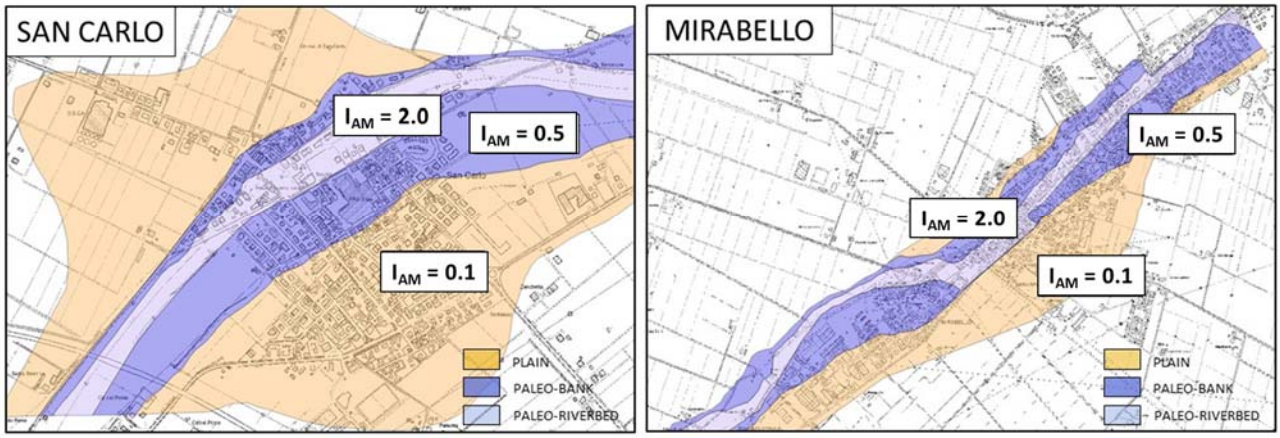

(**a**) (**b**)

Figure 14: Geological map with I_{AM} values adopted for the municipalities of San Carlo (**a**) and Mirabello (**b**).

Liquefaction fragility curves

In this section, preliminary liquefaction fragility curves are derived according to the methodologies described above for the entire dataset of buildings (i.e., about 750 in the NDL and DL classes and about 350 with no damage). Figure 15 reports the fragility curves for the assumed functional forms and fitting methodologies. Table 5 sets out the values of the estimated parameters for each fragility curve. Due to the reduced amount of data, no reliable estimation of the fragility curves at DG4 and DG5 can be provided.

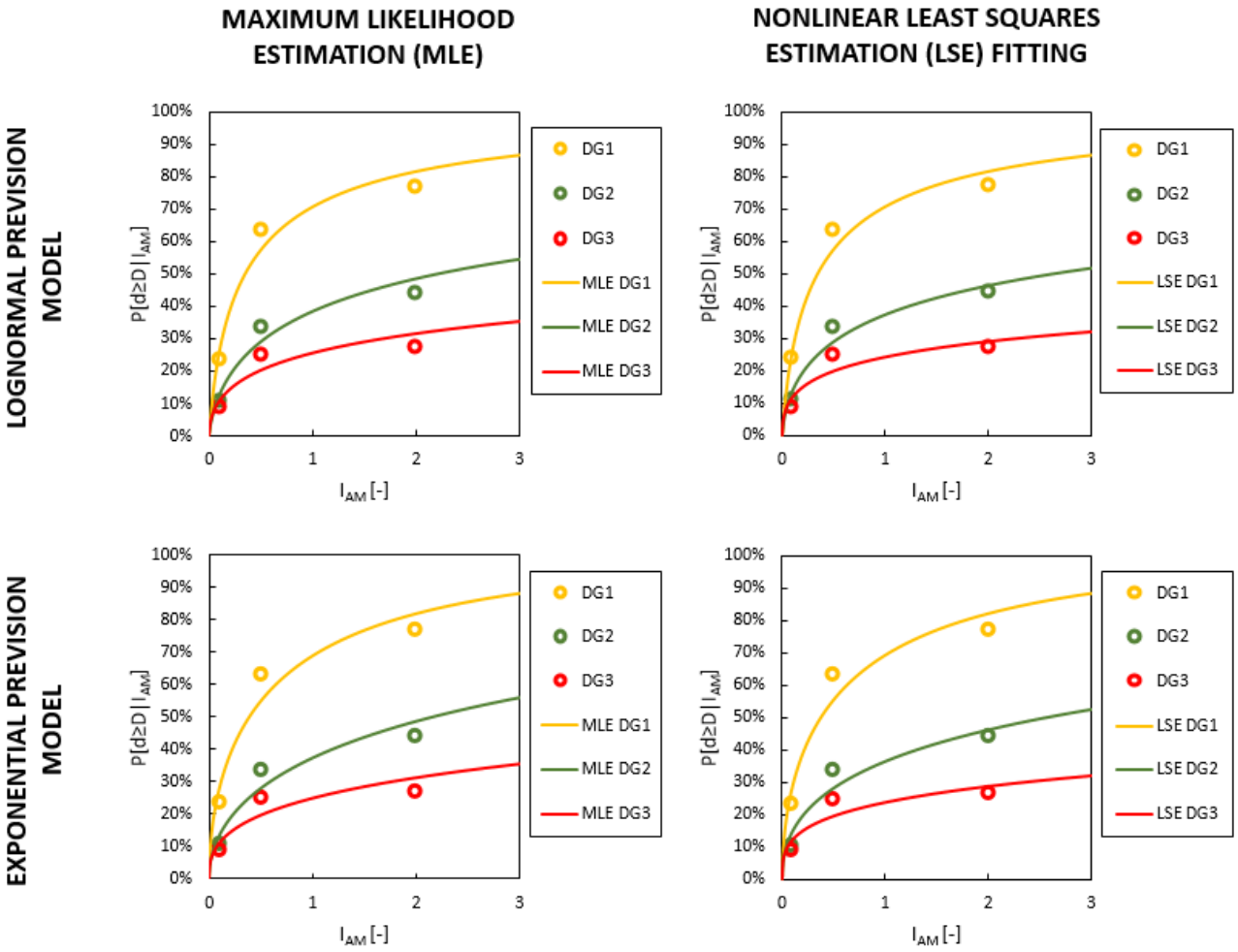

Figure 15: Lognormal and exponential fragility curves (*solid lines*) at different damage grades (DG) fitting observed fragility data (*circles*) for all the buildings and the adopted regression techniques (MLE and LSE).

Table 5: Lognormal and exponential fragility curve parameters for the damage states considered.

	DG1		DG2		DG3		
	μ	σ	μ	σ	μ	σ	
LSE	-1.07	1.99	0.96	2.99	3.29	4.71	Lognormal
MLE	-1.06	1.96	0.78	2.67	2.57	3.89	

	DG1		DG2		DG3		
	α	β	α	β	α	β	
LSE	1.17	0.53	0.45	0.45	0.27	0.32	Exponential
MLE	1.17	0.54	0.47	0.51	0.29	0.39	

Figure 15 shows that no significant difference is observed in the lognormal or exponential models. Strictly speaking, the advantages of using a functional form can be evaluated by comparing the values of: a) the weighted sum of the square of the errors in the LSE methodology; and b) the likelihood in the MLE methodology, obtained by adopting the lognormal and exponential models. In both cases, the use of the lognormal model yields slightly better results, i.e. a lower weighted sum of the square of the errors (with the LSE methodology) and a higher likelihood (with the MLE methodology).

CONCLUSIONS

The 2012 Emilia earthquake highlighted the large extent of the damage caused to structures and infrastructures due to soil liquefaction. The study presented herein investigated the effects of liquefaction on private residential masonry buildings using data on about 1,000 such structures located in several municipalities hit by the earthquake. According to empirical data collected immediately after the seismic event, it was possible to compare the behavior of structures whose soil foundation was not subjected to the liquefaction phenomena (the NDL class of buildings) with that of buildings that were (the DL class of buildings). The analysis of the damage in the DL class of buildings confirmed that, if immediately activated, liquefaction works as a natural isolation system against the transmission of inertial seismic actions on a superstructure; in these cases, the damage is mainly governed by the rigid rotation of buildings or settlements. However, liquefaction is often not immediately activated and this leads to a damage pattern that is characterized by both typical inertial damage (i.e., masonry walls overturning or in-plane cracks) and localized settlements (i.e. rigid rotation or one-way diagonal cracks).

The comparative analysis of the damage observed to the NDL and DL building classes has revealed evidence of the impact of soil liquefaction on structures. In particular, the empirical damage detected to the DL class of buildings was generally more severe than that sustained by the NDL class. The macro-parameters influencing the structural vulnerability of masonry buildings to inertial actions were less decisive in the evaluation of the global building damage caused by liquefaction. However, rigid horizontal structures confirmed their crucial role in limiting damage for both building classes. By using a model calibrated empirically to compute losses, the predicted repair costs were about 30% higher in the DL than the NDL buildings.

The correlation between structural damage and soil liquefaction allowed to derive empirical fragility curves as functions of a new parameter (I_{AM}), expressing the liquefaction demand because it is related to ground settlement, and therefore to structural damage. Under the simplified hypothesis that the uppermost liquefiable layer is fully liquefied (i.e. r_u=1), such a new liquefaction index can be calculated in a very straightforward way. In order to produce fragility curves to determine the

probability of exceeding the damage grades defined according to EMS-98, average values of I_{AM} were attributed to different parts of the two analysed villages, based on both in situ tests results and geological characteristics. Because of this simplification, in the next future a more detailed characterization of the villages will be done by carrying out more widespread in situ tests, obtaining therefore a more refined I_{AM} mapping. Although the curves presented herein depend on the local context where the seismic event occurred, and further data from other events are required, they certainly represent a preliminary tool to predict losses in liquefaction-prone areas and to establish priorities and reconstruction policies for use in the aftermath of future earthquakes.

Acknowledgments

This work has been carried out within the LIQUEFACT project. This project has received funding from the European Union's Horizon 2020 research and innovation programme under grant agreement No 700748. The activities reported in the paper were carried out within the framework of a scientific agreement between ReLUIS and the Emilia Romagna Region. We would like to recognize the crucial role of the "Seismic and Soil Geological Service" and in particular of Dr. Luca Martelli. We would also like to thank Mr. Pietro Caputo for his undergraduate thesis on the research topic presented in the paper and for his collaboration on the development of the analyses.

References

Adamidis O, Madabhushi SPG (2018) Deformation mechanisms under shallow foundations on liquefiable layers of varying thickness. Géotechnique, 68: 602-613.

Allmond J, Kutter BL, Bray J, Hayden C (2015) New Database for Foundation and Ground Performance in Liquefaction Experiments. Earthquake Spectra, 31(4), 2485–2509.

Amiri GG, Jalalian M, Amrei SAR (2007) Derivation of vulnerability functions based on observational data for Iran. In: Proceedings of international symposium on innovation and sustainability of structures in civil engineering, Tongji University, China

Baggio C, Bernardini A, Colozza R, Coppari S, Corazza L, Della Bella M, Di Pasquale G, Dolce M, Goretti A, Martinelli A, Orsini G, Papa F, Zuccaro G (2007) Field manual for post-earthquake damage and safety assessment and short-term countermeasures (Pinto A, Taucer Feds), Translation from Italian: Goretti A, Rota M, JRC Scientific and technical reports, EUR 22868 EN-2007; Available at: https://www.eeri.org/wp-content/uploads/Italy/EUR%2022868%20(2007)%20Field%20Manual%20for%20post-earthquake%20damage%20assessment.pdf

Baker JW (2015) Efficient analytical fragility function fitting using dynamic structural analysis. Earthq Spectra 31(1):579–599

Balakrishnan A, Kutter BL (1999) Settlement, sliding, and liquefaction remediation of layered soil. Journal of Geotechnical and Geoenvironmental Engineering, 125 (11):968-978.

Borzi B, Pinho R, Crowley H (2008) Simplified pushover-based vulnerability analysis for large scale assessment of RC buildings. Eng Struct 30(3):804–820

Bouckovalas GD, Karamitros DK, Madabhushi GSP, Cilingir U, Papadimitriou AG, Haigh SK (2015) FLIQ: Experimental verification of shallow foundation performance under earthquake-induced liquefaction. Geotechnical, Geological and Earthquake Engineering, 35:525-542.

Boulanger RW, Idriss IM (2016) CPT-Based Liquefaction Triggering Procedure. Journal of Geotechnical and Geoenvironmental Engineering, 142(2):04015065.

Bray JD Dashti S (2014) Liquefaction-induced building movements. Bulletin of Earthquake Engineering, 12: 1129-1156.

Calvi GM (1999) A displacement-based approach for vulnerability evaluation of classes of buildings. J Earthq Eng 3(3):411–438

Caputo P, Chiaradonna A, di Ludovico M, Bilotta E, Prota A, Flora A, Martelli L (2019). Soil liquefaction and induced damage to structures: a case study from the 2012 Emilia earthquake. Proceedings of the 7th International Conference on Earthquake Geotechnical Engineering, 7ICEGE, 17-20 June 2019, Rome, ISBN: 978-0-367-14328-2 (Hbk), eISBN: 978-0-429-03127-4 (eBook)

Cazares U, Nino M, Reinoso E (2012) Vulnerability functions for buildings due to liquefaction. Proceedings of the 15th World Conference on Earthquake Engineering (15WCEE), Lisboa, Portugal.

Chiaradonna A, Bilotta E, d'Onofrio A, Flora A, Silvestri F (2018a) A simplified procedure for evaluating post-seismic settlements in liquefiable soils. Proceedings of the 5th Conference on Geotechnical Earthquake Engineering and Soil Dynamics (GEESDV), Austin (TX), GSP 290:51-59. DOI: 10.1061/9780784481455.005

Chiaradonna A, Tropeano G, d'Onofrio A, Silvestri F (2018b) Interpreting the deformation phenomena of a levee damaged during the 2012 Emilia Earthquake. Special Issue of Soil Dynamic and Earthquake Engineering, SDEE, https://doi.org/10.1016/j.soildyn.2018.04.039

Cosenza E, Manfredi G, Polese M, Verderame GM (2005) A multi-level approach to the capacity assessment of existing RC buildings. J Earthq Eng 9(1):1–22

Crowley H, Pinho R, Bommer JJ (2004) A probabilistic displacement-based vulnerability assessment procedure for earthquake loss estimation. Bull Earthq Eng 2(2):173–219

Cubrinovski M (2013) Liquefaction-Induced Damage in The2010-2011 Christchurch (New Zealand) Earthquakes, Seventh International Conference on Case Histories in Geotechnical Engineering.

Dashti S, Bray JD (2013) Numerical Simulation of Building Response on Liquefiable Sand. Journal of Geotechnical and Geoenvironmental Engineering, 139(8): 1235-1249.

573 Del Gaudio C, Ricci P, Verderame GM, Manfredi G (2015) Development and urban-scale application
574 of a simplified method for seismic fragility assessment of RC buildings. Eng Struct 91:40–57. doi:
575 10.1016/j.engstruct.2015.01.031

576 Del Gaudio C, De Martino G, Di Ludovico M, Manfredi G, Prota A, Ricci P, Verderame GM (2017)
577 Empirical fragility curves from damage data on RC buildings after the 2009 L'Aquila earthquake.
578 Bulletin of Earthquake Engineering, Volume 15, Issue 4, 2017, Pages 1425-1450 DOI
579 10.1007/s10518-016-0026-1

580 De Martino G, Di Ludovico M, Prota A, Moroni C, Manfredi G, Dolce M (2017) Estimation of Repair
581 Costs for RC and Masonry Residential Buildings Based on Damaged Data Collected by Post-
582 Earthquake Visual Inspection, Bulletin of Earthquake Engineering, Volume 15, Issue 4, 2017, Pages
583 1681-1706, DOI 10.1007/s10518-016-0039-9.

584 Del Vecchio C, Di Ludovico M, Pampanin S, Prota A. (2018) Repair costs of existing RC buildings
585 damaged by the L'Aquila earthquake and comparison with FEMA P-58 predictions. Earthquake
586 Spectra. February 2018, Vol. 34, No. 1, pp. 237-263. DOI: 10.1193/122916EQS257M.

587 Di Ludovico M, Prota A, Moroni C, Manfredi G, Dolce M (2017a) Reconstruction process of
588 damaged residential buildings outside the historical centres after L'Aquila earthquake—part I: ''light
589 damage'' reconstruction. Bull Earthq Eng. doi:10.1007/s10518-016-9877-8

590 Di Ludovico M, Prota A, Moroni C, Manfredi G, Dolce M (2017b) Reconstruction process of
591 damaged residential buildings outside historical centres after the L'Aquila earthquake—part II:
592 ''heavy damage'' reconstruction. Bull Earthq Eng. doi:10.1007/s10518-016-9979-3

593 Dolce M, Moroni C, Samela C, Marino M, Masi A, Vona M (2001) Una Procedura di
594 Normalizzazione del Danno per la Valutazione degli Effetti di Amplificazione Locale, Proceedings
595 of the X National con-ference of seismic engineering in Italy, Potenza-Matera, 9-13 September (in
596 Italian)

597 Dolce M, Speranza E, Giordano F, Borzi B, Bocchi F, Conte C, Di Meo A, Faravelli M, Pascale V
598 (2017) Da.D.O - Uno strumento per la consultazione e la comparazione del danno osservato relativo
599 ai più significativi eventi sismici in Italia dal 1976, ANIDIS 2017 - XVII Convegno Pistoia 17
600 settembre 2017 – 21 settembre 2017.
601
602 Facciorusso J, Madiai C, Vannucchi G (2012) Rapporto sulla risposta sismica locale e pericolosità di
603 liquefazione a S. Carlo e Mirabello. http://ambiente.regione.emilia-
604 romagna.it/geologia/temi/sismica/liquefazione-gruppo-di-lavoro
605
606 Fioravante V, et al. (2013) Earthquake Geotechnical engineering aspects of the 2012 Emilia-
607 Romagna earthquake (Italy). Proceedings of the 7th International Conference on case Histories in
608 Geotechnical Engineering. pp. 1–34.

609 GNDT, (1993) Seismic Risk of Public Buildings, Part I: Methodology. Tipografia Moderna,
610 Bologna, Italy (in Italian)
611

612 Grünthal G (1998) Cahiers du Centre Européen de Géodynamique et de Séismologie: volume 15—
613 European Macroseismic Scale 1998. European Center for Geodynamics and Seismology,
614 Luxembourg

615 Gruppo di lavoro per la valutazione degli effetti di liquefazione a seguito dei terremoti del 20 e 29
616 maggio 2012 (Regione Emilia-Romagna, PG.2012.0134978 del 31/5/2012), Rapporto sugli effetti
617 della liquefazione osservati a Mirabello (Provincia di Ferrara), Dipartimento Protezione Civile e
618 Regione Emilia Romagna. http://ambiente.regione.emilia-
619 romagna.it/geologia/temi/sismica/speciale-terremoto/interventi-per-la-ricostruzione-e-la-ripresa
620
621 Hayden CP, Zupan JD, Bray JD, Allmond JD, Kutter BL (2015) Centrifuge tests of adjacent mat-
622 supported buildings affected by liquefaction. Journal of Geotechnical and Geoenvironmental
623 Engineering, 141(3).
624
625 Hughes FE, Madabhushi SPG (2019) Liquefaction induced displacement and rotation of structures
626 with wide basements. Soil Dynamics and Earthquake Engineering, 120: 75-84.
627
628 Iervolino I, Manfredi G, Polese M, Verderame GM, Fabbrocino G (2007) Seismic risk of R.C.
629 building classes. Eng Struct 29(5):813–820

630 Ishihara K (1985). Stability of natural deposits during earthquakes. Proceedings 11th International
631 Conference on Soil Mechanics and Foundation Engineering, 1: 321-376.

632 ISTAT (2011) 15° Censimento della popolazione e delle abitazioni 2011. Istituto Nazionale di
633 Statistica. http://www.istat.it/it/censimento-popolazione/censimento-popolazione-2011

634 Iwasaki T, Arakawa T, Tokida K (1984) Simplified Procedures for Assessing Soil Liquefaction
635 During Earthquakes. Soil Dynamics and Earthquake Engineering, 3(1):49–58.

636 Karamitros DK, Bouckovalas GD, Chaloulos YK (2013) Seismic settlements of shallow foundations
637 on liquefiable soil with a clay crust. Soil Dynamics and Earthquake Engineering, 46, pp.64–76.
638 Available at: http://dx.doi.org/10.1016/j.soildyn.2012.11.012.

639 Kutter BL, Gajan S, Balakrishnan A, Manda KK (2004) Effects of Layer Thickness and Density on
640 Settlement and Lateral Spreading. Journal of Geotechnical and Geoenvironmental Engineering,
641 ASCE, 130(6): 603-614

642 Lai CG, et al. (2015) Soil liquefaction during the 20 may 2012 M5.9 Emilia earthquake, Northern
643 Italy: Field reconnaissance and post-event assessment. Earthquake Spectra, 31(4):2351–2373.

644 Lopez-Caballero F, Khalil C (2018) Vulnerability Assessment for Earthquake Liquefaction–Induced
645 Settlements of an Embankment Using Gaussian Processes. ASCE-ASME Journal of Risk and
646 Uncertainty in Engineering Systems, Part A: Civil Engineering, 4(2):04018010. Available at:
647 http://ascelibrary.org/doi/10.1061/AJRUA6.0000957.

648 Luque R, Bray JD (2017) Dynamic Analyses of Two Buildings Founded on Liquefiable Soils during
649 the Canterbury Earthquake Sequence. Journal of Geotechnical and Geoenvironmental Engineering,
650 143(9):04017067. Available at: http://ascelibrary.org/doi/10.1061/%28ASCE%29GT.1943-5606.0001736.

651 Modoni G, Spacagna RL, Paolella L, Salvatore E, Rasulo A, Martelli L (2019) Liquefaction risk
652 assessment: lesson learned from a case study. Proceedings of the VII International Conference on
653 Earthquake Geotechnical Engineering, Roma (Italy), 17-20 June 2019. ISBN: 978-0-367-14328-2
654 (Hbk), eISBN: 978-0-429-03127-4 (eBook)

655 Morga M, Spacagna RL, Jones K, Modoni G (2018) Natural risk analysis of the built environment:
656 understanding strengths and weaknesses of both quantitative and qualitative methodologies. A case
657 study of soil liquefaction. 8th International Conference on Building Resilience – ICBR Lisbon'2018
658 Risk and Resilience in Practice: Vulnerabilities, Displaced People, Local Communities and Heritages
659 14-16 November 2018 – Lisbon, Portugal

660 Ordinanza n. 29 del 28 agosto 2012 Regione Emilia-Romagna, Criteri e modalità di assegnazione di
661 contributi per la riparazione e il ripristino immediato di edifici e unità immobiliari ad uso abitativo
662 danneggiati dagli eventi sismici del 20 e 29 maggio 2012 e temporaneamente o parzialmente inagibili.
663 Ordinanza Commissario Delega Regione Emilia- Romagna n.29 del 28/08/2012.
664 http://ambiente.regione.emilia-romagna.it/geologiatemi/ sismica/speciale-terremoto
665
666 Ordinanza n. 51 del 5 ottobre 2012 Regione Emilia-Romagna, Criteri e modalità di assegnazione di
667 contributi per la riparazione e il ripristino con miglioramento sismico di edifici e unità immobiliari
668 ad uso abitativo che hanno subito danni significativi dagli eventi sismici del 20 e 29 maggio 2012 e
669 che sono stati dichiarati inagibili. (ESITO E0). Ordinanza Commissario Delega Regione Emilia-
670 Romagna n. 51 del 5/10/2012. http://ambiente.regione.emilia-romagna.it/geologia/temi/
671 sismica/speciale-terremoto
672
673 Ordinanza n. 86 del 6 dicembre 2012 Regione Emilia-Romagna, Criteri e modalità di assegnazione
674 di contributi per la riparazione, il ripristino con miglioramento sismico o la demolizione e
675 ricostruzione di edifici e unità immobiliari ad uso abitativo che hanno subito danni gravi a seguito
676 degli eventi sismici del 20 e 29 maggio 2012 e che sono stati dichiarati inagibili (ESITO E1, E2 o
677 E3). Ordinanza Commissario Delega Regione Emilia-Romagna n.86 del 6/12/2012.
678 http://ambiente.regione.emilia-romagna.it/geologia/temi/sismica/speciale-terremoto
679 Papathanassiou G et al. (2015) Assessment of liquefaction potential for two liquefaction prone areas
680 considering the May 20, 2012 Emilia (Italy) earthquake. Engineering Geology, 189:1–16.
681 http://dx.doi.org/10.1016/j.enggeo.2015.02.002.

682 Rashidian V, Gillins DT (2018) Modification of the liquefaction potential index to consider the
683 topography in Christchurch, New Zealand. Engineering Geology, 232:68–81. Available at:
684 https://doi.org/10.1016/j.enggeo.2017.11.010.

685 Rossetto T, Elnashai A (2003) Derivation of vulnerability functions for European-type RC structures
686 based on observational data. Eng Struct 25(10):1241–1263

687 Rossetto T, Ioannou I, Grant DN (2013) Existing empirical fragility and vulnerability functions:
688 compendium and guide for selection. GEM technical report 2013-X, GEM Foundation, Pavia

689 Rota M, Penna A, Strobbia CL (2008) Processing Italian damage data to derive typological fragility
690 curves. Soil Dyn Earthq Eng 28(10):933–947

691 Sonmez H (2003) Modification of the liquefaction potential index and liquefaction susceptibility
692 mapping for a liquefaction-prone area (Inegol, Turkey). Environmental Geology, 44(7):862–871.

693 Sonmez H, Gokceoglu C (2005) A liquefaction severity index sUSgested for engineering practice.
694 Environmental Geology, 48(1):81–91.

695 Spacagna RL, Rasulo A, Modoni G (2017) Geostatical Analysis of Settlements Induced by
696 Groundwater Extraction. Proceedings of the 17th International Conference Computational Science
697 and its Applications, Trieste, Italy, July 3–6, 2017. Part IV LNCS 10407, pp. 350-364. DOI:
698 10.1007/978-3-319-62401-3_26

699 Spacagna RL, Paolella L, Rasulo A, Modoni G (2018) Spatial varibility of cpt data for liquefaction
700 assessment. Proceedings of the16th European Conference on Earthquake Engineering, Thessaloniki,
701 18-21 June 2018.

702 Tokimatsu K, Mizuno H, Kakurai M (1996). Building damage associated with geotechnical problems.
703 Special Issue of Soils and Foundations, 219-234.

704 Tropeano G, Chiaradonna A, d'Onofrio A, Silvestri F (2019) A numerical model for non-linear
705 coupled analysis on seismic response of liquefiable soils. Computers and Geotechnics, 105: 211-227.
706 https://doi.org/10.1016/j.compgeo.2018.09.008

707 Van Ballegooy S et al. (2014) Assessment of liquefaction-induced land damage for residential
708 Christchurch. Earthquake Spectra, 30(1):31–55.

709 Yoshida N, Tokimatsu K, Yasuda S, Kokusho T, Okimura T (2001) Geotechnical aspects of damage
710 in Adapazari city during 1999 Kocaeli, Turkey earthquake. Soils and Foundations, 41(4):25-45.

711 Zhang G, Robertson PK, Brachman RW (2002) Estimating liquefaction-induced ground settlements
712 from CPT for level ground. Canadian Geotechnical Journal, 39(5):1168–1180. Available at:
713 http://www.nrcresearchpress.com/doi/abs/10.1139/t02-047.

714 Zhang J, Huo Y, Brandenberg SJ, Kashighandi P (2008) Effects of Structural Characterizations on
715 Fragility Functions of Bridges Subject to Seismic Shaking and Lateral Spreading. Earthquake
716 Engineering and Engineering Vibrations. 7(4):369-382

717